IT-200PM Ring-Cusp Ion Thruster

IEPC-2019-339

Presented at the 36th International Electric Propulsion Conference
University of Vienna • Vienna, Austria
September 15-20, 2019

M.Selivanov[1] and A.Lovtsov[2]
Keldysh Research Centre, Moscow, 125438, Russian Federation

Abstract: This article gives an overview of design and first experimental results obtained on IT-200PM ring-cusp ion thruster. The IT-200PM discharge chamber is designed to provide three magnetic field configurations, which may be quickly interchanged using three different permanent magnet sets. Ring-cusp IT-200PM has demonstrated discharge voltage and beam flatness improvement and slight discharge loss worsening compared to its Kaufman prototype IT-200. Discharge voltage decreased from 30 to 28 V, beam flatness increased by 37% and discharge loss increased by 7%. It is expected, that discharge loss could be improved in the future by optimization of the magnetic flux density in the discharge chamber.

Nomenclature

Bcc	=	maximum closed contour inside discharge chamber;
F_B	=	beam flatness parameter;
j	=	ion beam current density;
j_{max}	=	maximal ion beam current density;
j_{min}	=	minimal ion beam current density;
j_{avg}	=	average ion beam current density;
r	=	distance from the thruster axis;
R	=	radius of the thruster;
I_d	=	discharge current;
U_d	=	discharge voltage;
I_b	=	beam current;
M_{Xe}	=	atom mass for xenon;
$\dot{m}$	=	total main and cathode mass flow rate;
e	=	electron charge.

I. Introduction

MODERN Russian GEO satellites actively employ Hall thruster based electric propulsion (EP) for North-South Station-Keeping. The specific impulse requirements of such satellites are constantly growing to provide improvement of payload fraction in the total spacecraft mass. As an example, platforms under development are to be equipped with KM-75 Hall thrusters with specific impulse of 2680 s at 810 V discharge voltage.[1] However this is likely to be the upper limit of specific impulse for Hall thrusters within the power class of <3 kW.[2,3] Further voltage increase leads to a set of problems regarding lifetime, discharge stability and thermal loads of a Hall thruster.

In this regard, development of an ion thruster (IT) of a 3kW power class is underway in Russia aimed for additional increase of GEO satellites EP specific impulse. Several design optimization tasks should be solved to make a worthy competition to the traditionally used Hall thrusters.

[1] Leading engineer, Department of Electrophysics, selivanov@kerc.msk.ru
[2] Chief of department, Department of Electrophysics, lovtsov@kerc.msk.ru.

Currently, one of the main problems of ion thrusters is high complexity of subsystem design, that leads to a decline in reliability and increases mass in comparison with Hall thrusters. Changing magnetic field design from Kaufman to ring-cusp is one of the possible steps towards the solution of the problem. This will result in significant thruster design simplification and weight reduction. As an example, NSTAR thruster built with ring-cusp magnetic system and actively used in space with a diameter of ion optics of 285 mm has a weight of only 8.2 kg.[4] Weight of a Kaufman thruster IT-200, mentioned in the article, is 10.5 kg with ion optics diameter of 200 mm.

In addition, using of ring-cusp discharge chamber also promises a simplification of the power supplies within the PPU because a solenoid power supply is no longer required.

High beam flatness is another advantage of a ring-cusp ion thruster. Beam flatness increase leads to the proximity to the theoretical limit of thrust density imposed by Child-Langmuir law. Thus, the required thrust would be achieved at the minimal ion optics surface area, hence at the minimal ion thruster size. Therefore, it allows further decrease of ion thrusters weight. The associated problem of ion optics lifetime caused by higher ion current density may be solved using grids made of carbon-based material.

II. IT-200PM design

The ring-cusp ion thruster is based on Kaufman IT-200 design.[5] To change the magnetic field design the discharge chamber with solenoids should be replaced by the chamber with permanent magnets. This was implemented in a new IT-200PM thruster.

IT-200PM discharge chamber wall has a conical and cylindrical sections welded together. Since the discharge chamber wall is an anode in ring-cusp design, the chamber was fitted with ceramic insulators to provide chamber wall electric insulation from the screen grid flange and from the cathode. To produce various magnetic field topology three or four ring-shape permanent magnets could be mounted on the discharge chamber wall externally.

IT-200PM also equipped by a simplified easily removable external casing. The rest of the thruster parts, such as ion optics, the cathode and the neutralizer are inherited from IT-200.

The appearance of IT-200PM is shown in Fig. 1 (a), discharge chamber with one of the magnetic system configuration – in Fig. 1 (b).

a)

b)
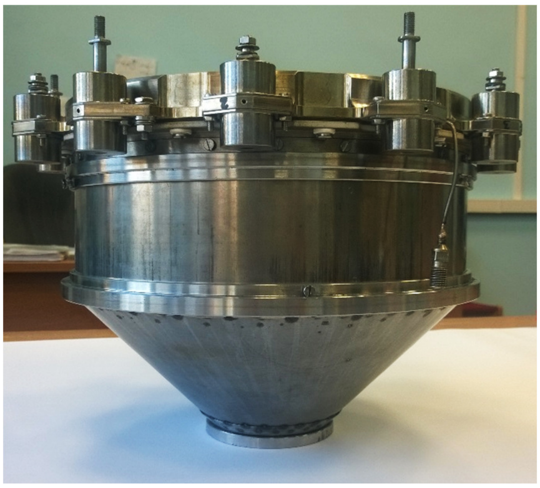

Figure 1. IT-200PM thruster:
a) the appearance, b) discharge chamber.

A. Magnetic system

The magnetic system of a ring-cusp ion thruster with 200 mm ion optics diameter was designed using the results of the studies of the other authors[6,7,8,9]. The analysis allowed to single out the main requirements to magnetic field parameters inside a ring-cusp discharge chamber:

- B_{cc}≈40 Gauss (an average of the values in Ref. 6 and 7);
- maximum discharge chamber volume with magnetic field under 10 Gauss;
- high magnetic field uniformity near the ion optics.

where B_{cc} is a maximum closed contour inside discharge chamber.

The calculation was carried out in FEMM software. Results of the calculation for three magnetic configurations are shown in Fig. 2:

- Configuration 1. Three cusps, B_{cc}≈40 Gauss. Intermediate magnet is placed on the cylindrical section of the discharge chamber;
- Configuration 2. Differs from Config.1 by placement of the intermediate magnet on the conic section instead of the cylindrical;
- Configuration 3. Four cusps, B_{cc}≈40 Gauss.

In view of the good results obtained by British scientists in a similar work[8] the ion optics pole made of a soft-core ferromagnetic from IT-200 was retained. This pole encloses magnetic field lines on itself weakening the magnetic field value in the region near the ion optics.

All configurations match the following criterions:

- B_{cc}≈40 Gauss (the fourth shade of gray from the down of the scale in the figure);
- the volume of the discharge chamber where the magnetic flux density is below 10 Gauss is significant;
- the magnetic flux density near the ion optics is less than 10 Gauss in all configurations, that corresponds to high field uniformity.

B. Magnetic field topology in the discharge chamber

Magnetic field measurements in the discharge chamber in the configuration 1, in absence of the cathode, the neutralizer cathode, casing and ion optics were held out to the define agreement of IT-200PM magnetic field topology and strength to the aforementioned calculated results. The measurements were performed with a Teslameter mounted on a positioning test bed with resolution of 0.01 mm. The Teslameter is capable operating with an A-probe for an axial component measurement and a T-probe for measuring a radial magnetic field component.

Radial and axial magnetic flux density components distributions are given in Fig. 3. The black continuous curve matches to the values acquired by calculation and the points represent experimental values. The distributions shown were obtained along a straight line running in a parallel to the discharge chamber axis (Z), in a distance of 100 mm from the latter. Zero position on Z-axis corresponds to the screen grid mounting plane.

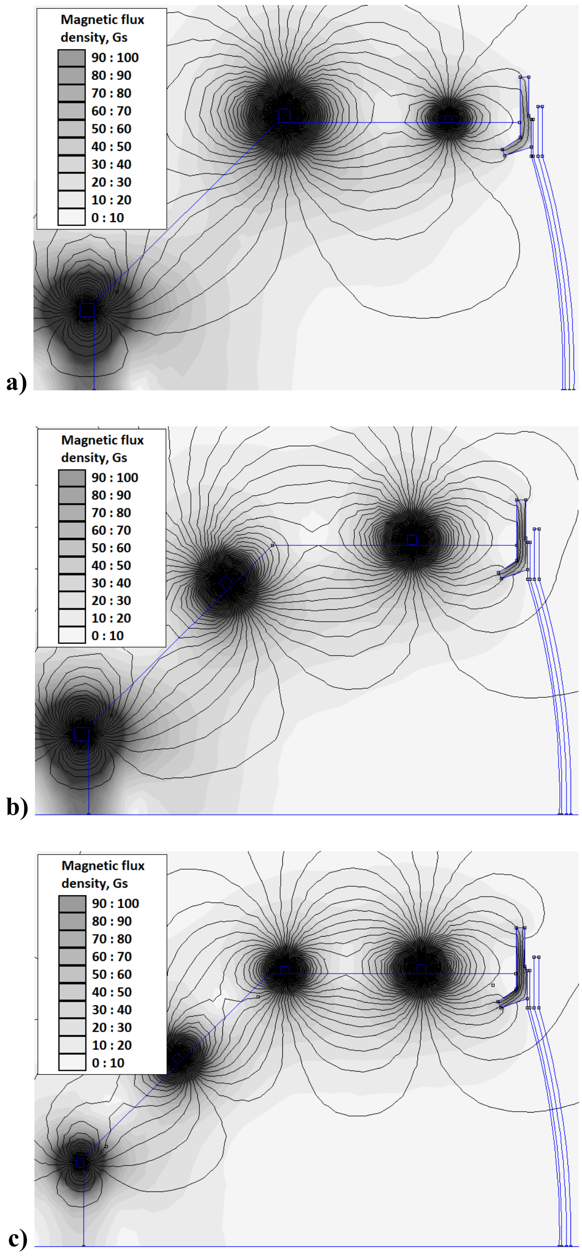

Figure 2. Magnetic field topology in IT-200PM for three magnetic system configurations: a) Configuration 1; b) Configuration 2; c) Configuration 3.

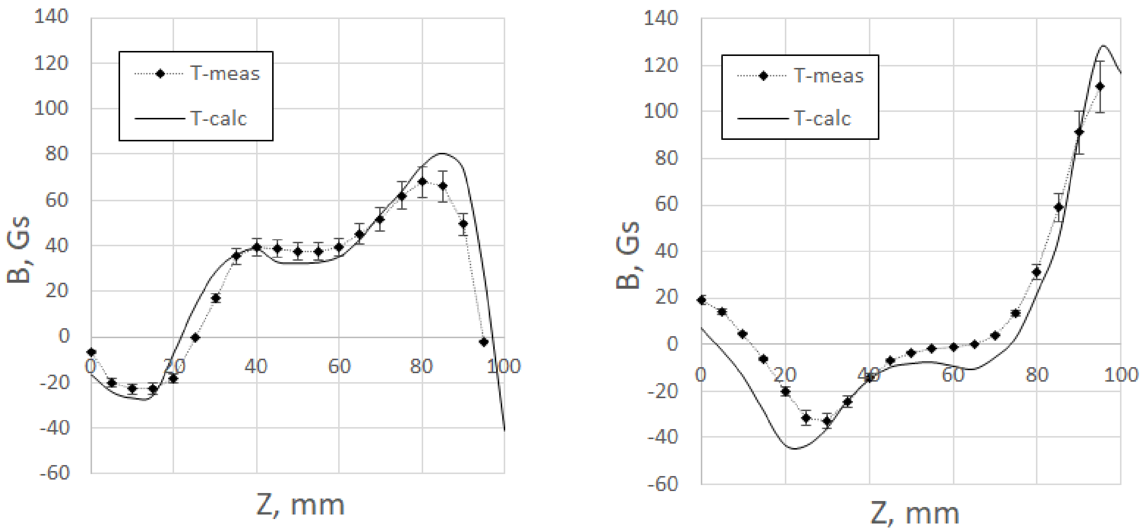

Figure 3. Comparison of the calculated and measured magnetic flux density: axial (left), radial (right).

As it can be seen from figure, the shape of the magnetic flux density curve acquired by calculation is in good agreement with the measurement results. The deviations occurring between the absolute values are related to the accuracy of the measurement and positioning apparatus, as well as with imprecision of magnet manufacturing and installation at the discharge chamber.

III. IT-200PM testing

A. Test equipment

The tests were performed in the cryovacuum facility[10] with the 90 m^3 volume and 3.8 m diameter vacuum chamber. The operating pressure in the chamber was less than $3\cdot10^{-3}$ Pa. The test facility electric system was used to power all the circuits of the thruster, including heaters and keepers of the cathode and neutralizer, the discharge, the accel grid and the screen grid. A system based on flow regulators with main flow rate of 2.7 mg/s, cathode flow rate of 0.5 mg/s and neutralizer flow rate of 0.5 mg/s was used. A system based on current and voltage sensors coupled with a LabVIEW computer data acquisition system was used to measure the electric parameters of the thruster.

The ion beam current density profile measurements were performed with five Faraday probes with the design suggested in Ref. 11. The probes were placed on a frame shaped as an arc equidistant to the ion optics, so that the distance from the accel grid to the collector surface was the same value for each of the five probes equal to 25 mm. The collector diameter was 10 mm. The Faraday probe schematics is shown in Fig. 4.

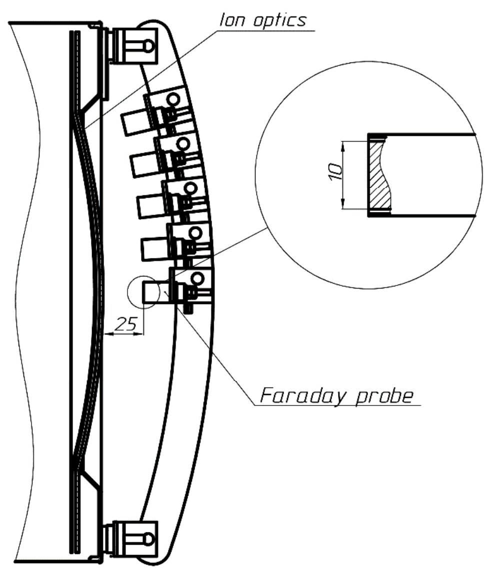

Figure 4. The Faraday probe schematics.

Extracting the beam while the frame with the Faraday probes is mounted on the thruster for over 10 minutes caused probe overheating and affected the parameters of the thruster. Therefore, the discharge chamber performance tests were held out separately from the measurements of ion beam current density profile.

A group of curves, each demonstrating a dependency of the discharge loss from mass utilization efficiency at a fixed discharge voltage is the result of the discharge chamber performance tests. The values of the voltage are being selected to cover that range of mass utilization efficiency between 0.85 and 0.95.

A thruster control system with two stabilizing circuits was used in the tests: the first sustained beam current of 1 A by adjusting the discharge current, the second kept a selected discharge voltage by regulating main flow rate. Consequently, an array of voltage and current values in the electric circuits, as well as the main and cathode flow rates was acquired. The data was used to calculate the discharge loss and the mass utilization efficiency in each of the operating modes, later used to build the performance curves.

The discharge loss is calculated as a ratio of the discharge power to the beam current. Since the electric circuit schematics is so that the beam current runs through the discharge circuits too, this power is subtracted from the total discharge power:

$$c_i = \frac{I_d \cdot U_d - I_b \cdot U_d}{I_b}$$

where:

I_d –discharge current;

U_d –discharge voltage;

I_b – beam current;

The mass utilization efficiency is determined by a relationship:

$$\eta_{md} = \frac{I_b \cdot M_{Xe}}{\dot{m} \cdot e}$$

where:

M_{Xe} – Xenon atom mass;

$\dot{m}$ – total main and cathode mass flow rate;

e – electron charge.

The ion beam current density profile measurements were performed separately, after opening the vacuum chamber and mounting the Faraday probe system on the thruster. At that, the thruster operation modes completely matched those studied earlier to determine the performance curves. Each probe was connected to the "Ground" clamp with an amperemeter adopted into the circuit to measure the ion current density radial profiles. The amperemeter readings were the results determined in the measurement. A power source providing probe collector potential of minus 30 V was connected to the circuit in series to cut out the beam plasma electrons.

B. Discharge chamber performance

The tests to determine performance of IT-200PM discharge chamber were carried out at the screen grid voltage of 4500 V, accel grid voltage of minus 400 V and the beam current of 1 A. Cathode keeper current was zero in all the modes and the neutralizer keeper current was 1 A. The discharge voltage and cathode mass flow rate were altered in order to get the discharge chamber performance curves.

Only two cathode flow rates for each value of the discharge voltage were used in tests in the Configuration 3, unlike the Configurations 1 and 2. This is due to discharge instability at other cathode flow rates, so that the discharge voltage oscillations occur with an amplitude of 3 V. The given magnitude of oscillations corresponds to measurements with frequency of 5 Hz.

Graphs of the discharge loss of the ring-cusp discharge chamber as a function of the mass utilization efficiency are given in Fig. 5a – 5c for the configurations 1 – 3 respectively. Comparison of the best modes for the ring-cusp and Kaufman discharge chambers is presented in Fig. 5d. There were no measurements of doubly charged ions during the tests and the current of screen grid was used as the beam current in mass utilization efficiency calculation. Thus, mass utilization efficiency for number of points exceeds 1,0 in the Fig. 5.

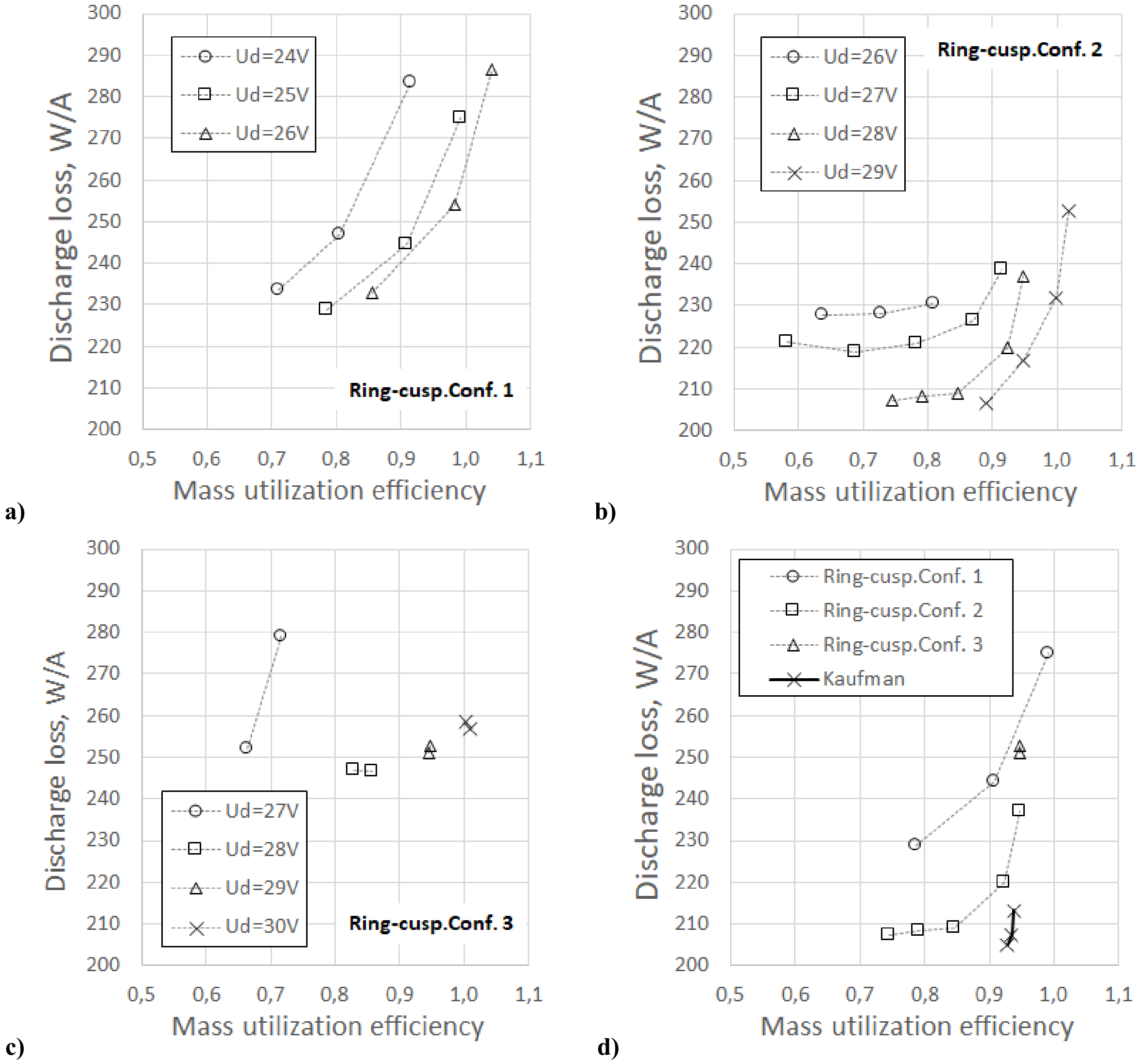

Figure 5. Discharge chamber performance curves for magnetic field designs: a) ring-cusp in the configuration 1, b) ring-cusp in the configuration 2, c) ring-cusp in the configuration 3, d) ring-cusp and Kaufman.

The best operation modes of a ring-cusp discharge chamber are achieved in the lower right part of efficiency curves[12] and lay in the range of 0.85 to 0.95. Lesser values do not offer high thruster specific impulse and decrease the lifetime of ion optics and thruster as a whole. At higher values the fraction of double-charged ions grows reducing thrust at fixed electric parameters of a beam. The discharge chamber performance parameters, providing the required range of mass utilization efficiency, are presented in table 1.

Table 1. Performance parameters of ring-cusp and Kaufman discharge chambers

Magnetic system	Discharge loss, W/A	Mass utilization efficiency	Discharge voltage, V
Ring-cusp config.1	244	0.91	25
Ring-cusp config.2	220	0.92	28
Ring-cusp config.3	251	0.95	29
Kaufman	205	0.93	30

It is shown in the table that discharge loss of the ring-cusp discharge chamber is higher than one of the Kaufman discharge chamber in all magnetic field configurations and operation modes. However, required values of mass utilization efficiency are achieved at lower discharge voltages. Besides, the difference in the discharge loss for the configuration 2 is ~7%.

The thing that is also to be taken into consideration is that the Kaufman discharge chamber performance parameters were achieved at the optimal magnetic field flux density, which was found in the tests by adjusting coil current. Magnetic field optimization in case of a ring-cusp discharge chamber demands to carry out a series of experiments for each configuration with several subconfigurations with the same magnetic field topology but different values of magnetic flux density. The subconfiguration can only be implemented by equipping different sets of permanent magnets. Manufacturing of such magnets sets and test procedures are long and complex. Thus, the magnetic field value optimization tests were not carried out in the scope of this work.

So, the ring-cusp discharge chamber performance may be enhanced as compared to the obtained results by altering the absolute value of the magnetic flux density in the course of further optimization.

C. Beam flatness

Another important performance factor of a discharge chamber, which affects the lifetime and thrust throttling range, is the beam flatness. It is usually evaluated by beam flatness parameter equal to the ratio of average ion current density to the peak value over the ion optics:

$$\eta = \frac{j_{avg}}{j_{max}},$$

where the average value of the current density is given by the following relationship:

$$j_{avg} = \frac{\int_0^R 2\pi r \cdot j(r)dr}{\pi R^2}.$$

The beam flatness affects the lifetime and thrust throttling range by a following mechanism.

Ion thruster lifetime is determined chiefly by the accel grid wear rate. The wear occurs by bombardment of the grid with slow secondary ions produced in a process of fast ion charge exchange with propellant atoms present in the gap between grids and near the external surface of the accel grid. Low beam flatness parameter corresponds to high peak current density of the accelerated ions and as well, the rate of secondary ion production, thus the erosion rate is higher in this region.

Thrust throttling is usually achieved by throttling the beam current at fixed beam voltage. The current throttle ratio is determined by two factors: ion current density range available for a grids aperture and flatness of the beam current density profile. Circular ion optics apertures usually offer a wide range of current density, which is 8 to 150 A/m^2 in case of IT-200PM. However, in the design used, the geometric parameters of an aperture are the same for all the ion optics area, and so the low beam flatness parameter results in narrowing the range of thrust throttling. The lower limit of this range is defined by extraction of beams from apertures on the periphery of the ion optics, and the upper limit is defined by extraction from apertures in the center of the ion optics.

It should be noted that some ion thrusters, for example, NSTAR has no lower limit for aperture ion current density.[13] In this case, the throttling range is defined by the beam flatness parameter only. In thrusters which has the lower limit of current density, IT-200PM ion optics for instance, it is important not only to secure high beam flatness parameter, but to provide a low value of a ratio of the average current density to the minimal one.

Fig. 6a – 6c show the results of beam current density profiles measurements in configurations 1 – 3 respectively. The horizontal axis of the graphs is the radial distance from the measurement point to the thruster axis, while the vertical axis is the beam current density normalized to the value on the thruster center line. The dot lines show the profiles of the beam current density obtained in each operation mode separately, the solid line shows the beam current density profile averaged through all operation modes. In Fig. 6d, the averaged profiles of the beam current density for the three different ring-cusp configurations and the corresponding profile for the Kaufman thruster are shown.

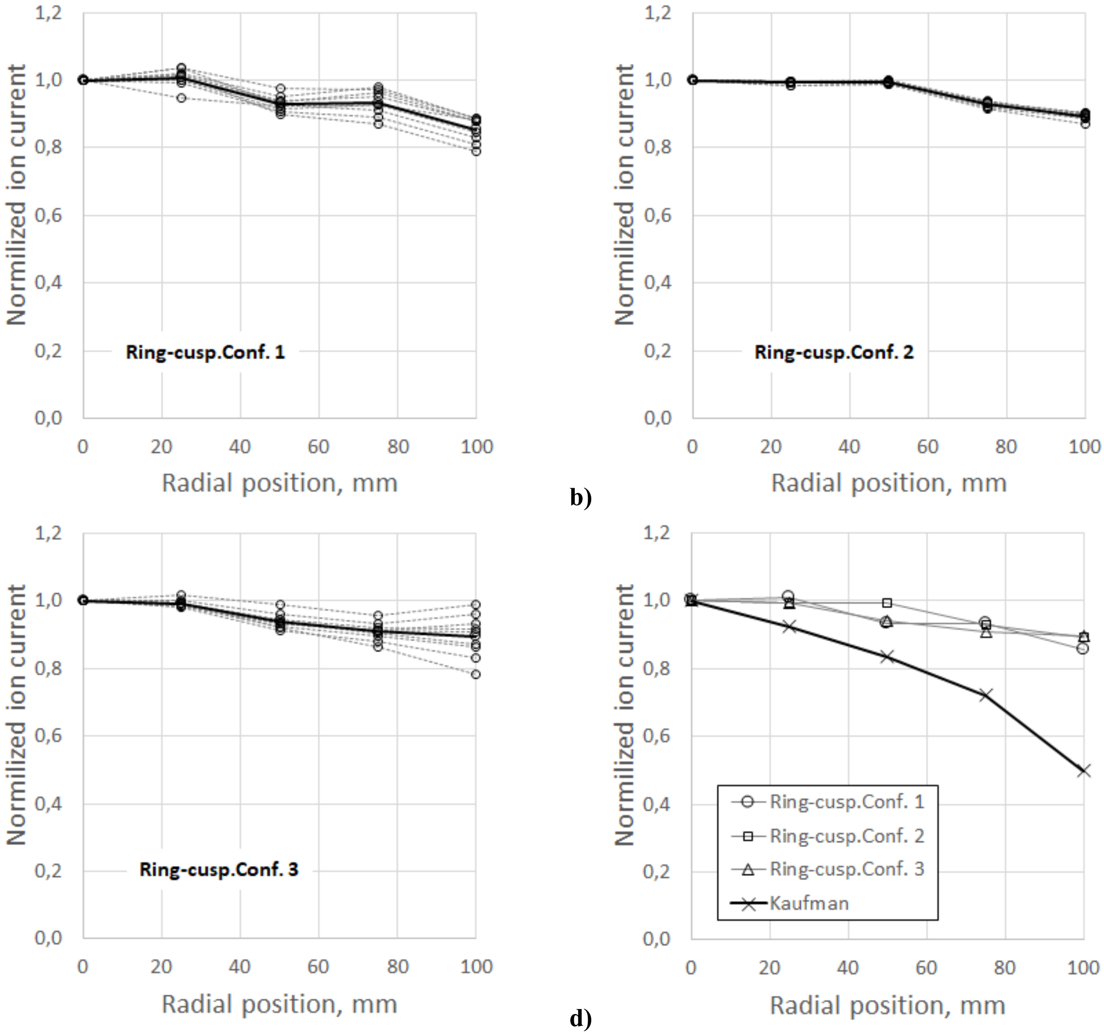

a) b) c) d)

Figure 6. Normalized beam current density profile: a) ring-cusp in the config.1, b) ring-cusp in the config.2, c) ring-cusp in the config.3, d) ring-cusp and Kaufman.

The difference in the shape of the current density profiles, observed in one of the configurations at various operation modes and chiefly common for the configuration 3, is likely to be associated with collector surface area change of Faraday probes in the course of their heating by the ion beam power. In fact, aside from the aforementioned discharge instability, the configuration 3 has another feature. It takes a longer time to achieve the stationary parameters since the beam extraction moment. It causes the probes to heat up to temperature of over 500°C, thus, possibly affects the magnitude of collected ion current. To make further estimations, the beam current density profiles averaged over all modes were used for each of the configurations. Beam flatness parameters corresponding to each beam current density profile in Fig. 6d are given in table 2.

Table 2. Beam flatness parameter of ring-cusp and Kaufman thrusters

Thruster	Ring-cusp Config.1	Ring-cusp Config.2	Ring-cusp Config.3	Kaufman
Beam flatness parameter	0.92	0.93	0.92	0.68

The table demonstrates that the ring-cusp discharge chamber exceeds the Kaufman discharge chamber in terms of beam flatness in all the studied magnetic configurations by a value of 37 %. This is a great advantage of the ring-cusp discharge chamber, since it allows creating ion thruster with greater lifetime and wider thrust throttling range.

Such a significant beam flatness difference between two discharge chamber types is likely associated with topology and value of the magnetic field inside the discharge chamber. Results of magnetic field topology calculations inside the ring-cusp and the Kaufman discharge chambers are shown in Fig. 7. The calculations were performed using Magnet2D software. The magnetic flux density is shown in color, the black curves diverging out of the poles are magnetic field lines.

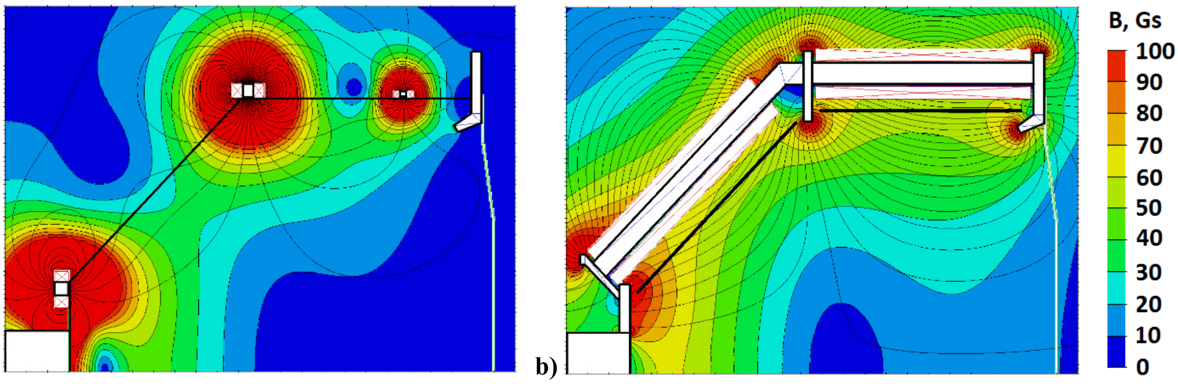

Figure 7. Magnitude and topology of magnetic field in the discharge chamber: a)PM in the config.1 (left), b) Kaufman (right).

As it can be seen from the figure, the ring-cusp discharge chamber has the minimum in the magnetic flux density covering the anode with a value of ~40 Gauss, while in the Kaufman discharge chamber this value exceeds 50 Gauss. Besides, the discharge chamber volume with weak magnetic field is much higher in case of the ring-cusp than in case of the Kaufman discharge chamber. Magnetic flux density distribution along the radius over the ion optics for the two discharge chamber types is given in Fig. 8.

The magnetic flux density in the periphery of the Kaufman discharge chamber is ~40 Gauss, while for the ring-cusp discharge chamber this value is under 5 Gauss all over the surface of the ion optics. Such field profile in ring-cusp discharge chamber must allow primary electrons, i.e. the electrons that flew out of the cathode, to reach the region near the ion optics freely. The primary electrons usually have energy exceeding ionization potential of propellant, thus they significantly affect on the distribution of the plasma density and the ion current density.

Calculation results of trajectories of primary electrons in magnetic field are presented in Fig. 9. Calculation was performed using Magnet2D software to make estimations of primary electron distributions in the volume of both types of discharge chamber.

The calculations were made for the following initial conditions:

- the electrons are emitted from the surface that corresponds to the keeper orifice of the cathode;
- the energy of the electrons is the same and equals to 20 eV;
- the influence of electric field on the electron motion is neglected;
- the influence of elastic collisions with other particles is neglected;
- elastic mirror reflection from surfaces with cathode potential;
- reflection from ion optics is elastic, approximately mirror (reflection angle may vary from the incidence angle by a value not exceeding 10 degrees*)

** This deviation is associated with the fact that the plasma border adjacent to apertures, which has approximately spherical shape at optimal focusing of accelerated ions, forms the bulk of the reflecting surface. The electron reflection conditions at ion optics are described in details in Ref. 14.*

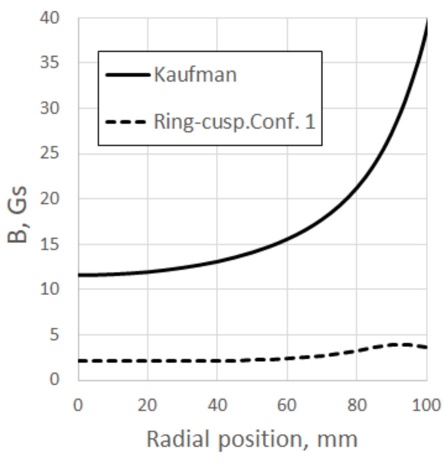

Figure 8. Magnetic flux density distribution along the radius.

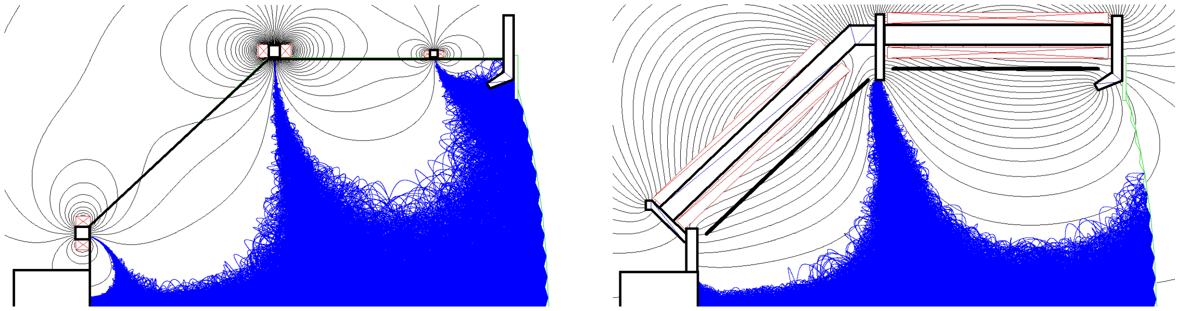

Figure 9. Primary electrons trajectories in discharge chamber: ring-cusp in config.1 (left), Kaufman (right).

The calculation results proved that the weak magnetic field near the ion optics founded in the ring-cusp discharge chamber allows primary electrons moving freely in this region. In Kaufman discharge chamber, all electron trajectories in the calculation are concentrated near the axis. This is likely defines the presence of the brightly manifested maximum of beam current density profile, that is typical for the Kaufman thrusters, and high beam flatness for the ring-cusp ion thrusters.

IV. Conclusion

This article describes the first results of calculations and experimental activities in the course of development of IT-200PM thruster with a ring-cusp discharge chamber. Experimental studies were carried out in two magnetic field configurations with three cusps and one with four cusps. Ring-cusp ion thruster has shown insignificant worsening in terms of discharge loss and great improvement in terms of discharge voltage and beam flatness in comparison with Kaufman thruster. In the best of the studied ring-cusp magnetic field configuration discharge loss increased by about 7%, discharge voltage decreased from 30 to 28 V and beam flatness increased by 37%. Calculation of discharge chamber electrons trajectories shown, that beam flatness parameter increase is connected to lower values of magnetic flux density near the ion optics.

References

[1]Lovtsov, A.S., Tomilin, D.A., Muravlev, V.A. "Development of High-Voltage Hall Effect Thrusters at Keldysh Research Centre", IAC-17.C4.4.4x39529, *68th International Astronautical Congress*, 2017.

[2]Manzella, D. H., Jacobson, D. T. and Jankovsky, R. S. "High Voltage SPT Performance", *37th Joint Propulsion Conference,* AIAA-2001-3774, Salt Lake City, UT, 2001.

[3]Pote, B. and Tedrake, R. "Performance of a high specific impulse Hall thruster", *27th International Electric Propulsion, Conference,* IEPC-01-35, Pasadena, CA, 2001.

[4]Christensen, J., Freick, K., et al. "Design and Fabrication of a Flight Model 2.3 kW Ion Thruster for the Deep Space 1 Mission", *37th Joint Propulsion Conference,* AIAA 98-3327, Cleveland, OH, USA, 1998.

[5]Lovtsov, A.S., Shagayda, A.A. "Ion Thrusters Development for a Transport and Power Generation Module Project", *34th International Electric Propulsion Conference,* IEPC-2015-291, Hyogo-Kobe, Japan, 2015.

[6]Wirz, R., Goebel, D. "Ion Thruster Discharge Performance per Magnetic Field Topography", *44th Joint Propulsion Conference*, AIAA 2006-4487, Pasadena, CA, 2006.

[7]Sengupta, A. "Experimental Investigation of Discharge Plasma Magnetic Confinement in the NSTAR Ion Thruster", *43th Joint Propulsion Conference*, AIAA 2005-4069, El Segundo, CA, 2005.

[8]Coletti, M., Wallace, N., Gabriel, S.B. "Ring Cusp Ion Engine Development in the UK", *34th International Electric Propulsion Conference,* IEPC-2015-130, Hyogo-Kobe, Japan, 2015.

[9]Ogunjobi, T.A. and Menart, J.A. "Computational Study of Ring-Cusp Magnet Configurations that Provide Maximum Electron Confinement". *44th Joint Propulsion Conference*, AIAA 2006-4489, Pasadena, CA, 2006.

[10]Gorshkov, O. A., Ilyin, A.A., Rizakhanov, R.N. "New Large Facility for High-Power Electric Propulsion Tests", *6th Propulsion for Space Transportation of the XXI Century Symposium*, Paper S20_2, France, 2002.

[11]Hofer, R., Walker, M., Gallimore, A. "A Comparison of Nude and Collimated Faraday Probes for Use with Hall Thrusters", *27th International Electric Propulsion Conference*, IEPC-01-020, Pasadena, CA, 2001.

[12]Goebel, D.M., Katz, I. *Fundamentals of Electric Propulsion: Ion and Hall Thrusters*, Wiley, California, USA, 2008.

[13]Gorshkov, O., Graphov, D., Muravlev, V., Shagayda, A. "The Results of Numerical and Experimental Investigation of Low-Power Ion Thruster with Slit-Type Acceleration System", ESASP-465, *Spacecraft Propulsion, Third International Conference*, p.459, 2000.

[14]Koroteev, A., Lovtsov, A., Muravlev, V., Selivanov, M., Shagayda, A. "Development of ion thruster IT-500", *The European Physical Journal D*, Vol. 71, №5, 2017.